Carbohydrate Polymers 95 (2013) 664–674

Contents lists available at SciVerse ScienceDirect

Carbohydrate Polymers

journal homepage: www.elsevier.com/locate/carbpol

# Thermoplastic starch films reinforced with talc nanoparticles

Luciana Castillo[a], Olivia López[a,b,*], Cintia López[a], Noemí Zaritzky[b], M. Alejandra García[b], Silvia Barbosa[a], Marcelo Villar[a]

[a] Planta Piloto de Ingeniería Química, PLAPIQUI (UNS-CONICET), Departamento de Ingeniería Química, UNS, Camino La Carrindanga km. 7, 8000 Bahía Blanca, Argentina

[b] Centro de Investigación y Desarrollo en Criotecnología de Alimentos, CIDCA (UNLP-CONICET), Facultad de Ciencias Exactas, UNLP, 47 y 116, 1900 La Plata, Argentina

ARTICLE INFO

*Article history:*
Received 28 November 2012
Received in revised form 4 March 2013
Accepted 5 March 2013
Available online xxx

*Keywords:*
Thermoplastic corn starch
Talc nanoparticles
Films
Thermo-compression
Characterization

ABSTRACT

Nanocomposite films of thermoplastic corn starch (TPS) with talc particles were obtained by thermo-compression in order to study the effect of filler on structure, optical, and thermal properties. Talc increased the films rigid phase, thus their cross-sections resulted more irregular. Talc preferential orientation within matrix and good compatibility between particles and TPS was observed by SEM. Slight crystalline structure changes in TPS matrix were measured by XRD and DSC, due to talc nucleating effect. Randomly dispersed talc nanoagglomerates and individual platelets were assessed by TEM. Laminar morphology and nano-sized particles allowed that nanocomposite films were optically transparent. TPS–talc films resulted heterogeneous materials, presenting domains rich in glycerol and others rich in starch. Talc incorporation higher than 3%, w/w increased softening resistance of the nanocomposites as stated by DMA. Relaxation temperatures of glycerol-rich phase shifted to higher values since talc reduces the mobility of starch chains.



## 1. Introduction

Mounting environmental and legislative pressure for reducing petroleum-based plastics waste and rapid increases in the petroleum price have primed the development of bio-based materials from renewable resources (Ma, Chang, Yu, & Stumborg, 2009). In this context, starch has received considerable attention because of its totally biodegradable nature, low cost and wide availability (López, García, & Zaritzky, 2008, 2010a,b; López, Lecot, Zaritzky, & García, 2011). Several studies reported the use of starches from different sources as raw material for films and coatings with different properties, showing the potential of this carbohydrate in these application fields (Avérous & Frigant, 2001; Famá, Flores, Gerschenson, & Goyanes, 2006; García, Martino, & Zaritzky, 2000; García, Pinotti, Martino, & Zaritzky, 2009; López et al., 2008, 2010a,b; López et al., 2011; Mali, Karam, Pereira Ramos, & Grossmann, 2004; Mali, Sakanaka, Yamashita, & Grossmann, 2005; Müller, Laurindo, & Yamashita, 2009). Native starch presents a granular structure, which can be disrupted and converted into thermoplastic starch (TPS) by processing under high temperature and shear conditions in presence of plasticizers (Halley et al., 2001; Ma et al., 2009; Pinto, Carbajal, Wypych, Ramos, & Satyanarayana, 2009). Nowadays, the research about the development of films based on TPS is promoted since starch can be processed employing the same technology used for synthetic polymers like extrusion, blowing, thermo-compression or injection molding (Parra, Tadini, Ponce, & Lugão, 2004; Tapia Blácido, Sobral, & Menegalli, 2005). This advantage allows the use of actual machinery, turning easier its processability and lowering industrial sector inversion. Unfortunately, TPS materials exhibit some disadvantages such as their strong hydrophilic character and poor mechanical and barrier properties compared to synthetic polymers (Avérous & Boquillón, 2004; Ma et al., 2009). An approach to overcome this limitation is to strengthen TPS matrixes with organic or mineral fillers (Cyras, Manfredi, Ton-That, & Vazquez, 2008). These fillers reinforce biopolymeric matrixes and led to develop films with special properties due to the synergic effect between the components (Wilhelm, Sierakowski, Souza, & Wypych, 2003). TPS–composite films have a potential use as packaging materials for food, cosmetics, and pharmaceutics products, among others. Lagaron and López-Rubio (2011) has stressed about the advantages of nanoclays inclusion in the formulation of active packaging based on bioplastics, which increase packaged foods quality and safety. As a consequence composites are developed to improve material mechanical performance, to ameliorate properties dependence on moisture, as well as, to prevent retrogradation of TPS based films. In general, the effective incorporation of filler particles within the matrix depends on the interaction strength between components.

* Corresponding author at: Planta Piloto de Ingeniería Química, PLAPIQUI (UNS-CONICET), Departamento de Ingeniería Química, UNS, Camino La Carrindanga km. 7, 8000 Bahía Blanca, Argentina. Tel.: +54 0291 4861700.
*E-mail address:* ovlopez75@yahoo.com.ar (O. López).

0144-8617/$ – see front matter © 2013 Elsevier Ltd. All rights reserved.
http://dx.doi.org/10.1016/j.carbpol.2013.03.026

Stronger filler–matrix interactions assure the homogenous incorporation of particles to the matrix; which results in improved ductility, strength, and optical properties among others.

Biopolymers reinforced with micro-sized fillers usually present some defects since they could act as stress concentrators affecting the mechanical performance of the final materials. This limitation is minimized as the particle size of the reinforcing agent diminishes (Ludueña, Alvarez, & Vasquez, 2007). In this sense, the development of biopolymer nanocomposites is rapidly emerging as a multidisciplinary research activity whose results could broaden polymer applications to the great benefit of different industries. Studies have shown that dispersing individual high aspect ratio silicate platelets leads to dramatic property enhancements, e.g. increased stiffness and strength, improved barrier properties, and better dimensional stability at very low filler concentrations (Fornes & Paul, 2003). Most of the works reported in the literature are related with starch matrixes containing different clays (Alexandre & Dubois, 2000; Chen & Evans, 2005; Cyras et al., 2008; Tunjano et al., 2009; Wilhelm et al., 2003). On the other hand, the use of talc as filler of TPS is an alternative scarcely investigated. Talc qualifies as good reinforcement filler of polymeric matrices because it is a layered mineral with a high aspect ratio (particle diameter/thickness ≈ 20:1). This is a consequence of its platy nature, having micron-sized dimensions on length and width, with nanometric thicknesses (Castillo, Barbosa, Maiza, & Capiati, 2011) Talc has an ideal formula of $Mg_3(Si_4O_{10})(OH)_2$; its elementary structure is comprised of an octahedral magnesium hydroxide sheet ($Mg_{12}O_{12}H_4$) sandwiched between two tetrahedral silica sheets ($SiO_2$), in order to form talc layers that are superimposed indefinitely. The size of an individual talc platelet (a few thousand of elementary layers) can vary from approximately 1 to over 100 μm, depending on the conditions of ore formation. van der Waals' gaps (interlayer or gallery) between the layers are formed due to stacking, which may assist in the delamination behavior of talc particles during the blending with TPS. Layer charge is zero or very small, as there are not ions present between layers.

The effects of talc on synthetic polymers have been large studied. It was demonstrated that talc improves mechanical properties and macromolecular orientation of polypropylene (Castillo, Barbosa, & Capiati, 2012). Moreover, an induced crystalline structure has been reported, suggesting that talc particles act as a nucleating agent for polymer crystallization (Castillo et al., 2012). Also, high aspect ratio platelets have been used to improve gas barrier properties. Typical polymer processing operations used in packaging lead to preferred orientation with the platelets aligned parallel to the surfaces. As a consequence, the aligned, overlapping platelet particles greatly increase the diffusion distance by creating a tortuous path for the diffusing species (Castillo et al., 2011). In addition, talc is also chemically inert and water repellent. This is a very important aspect when the mineral filled packaging material comes in contact with food which often includes acids and oils for flavor/taste purposes, increased shelf life, etc. These ingredients need to stay within the food and they should not migrate through the package wall.

The aims of this work are to develop nanocomposite films based on thermoplastic corn starch with talc nanoparticles and to evaluate the effect of filler addition on the structure and properties of TPS–talc nanocomposite films.

## 2. Materials and methods

### 2.1. Materials

Native corn starch was provided by Misky-Arcor (Tucumán, Argentina) with an amylose content of 23.9 ± 0.7% (López et al., 2008). Talc sample was supplied by Dolomita SAIC (Argentina). This mineral comes from an Australian ore, having a high purity (98%), median size d50 of 5.9 ± 3.8 μm (particle size at which 50% of the population resides above this point and half resides below this point) and nanometric thickness of 79 ± 16 μm. Fig. 1 includes a SEM micrograph in order to show the morphology and size of talc particles. Glycerol (Anedra, Argentina) was used as plasticizer.

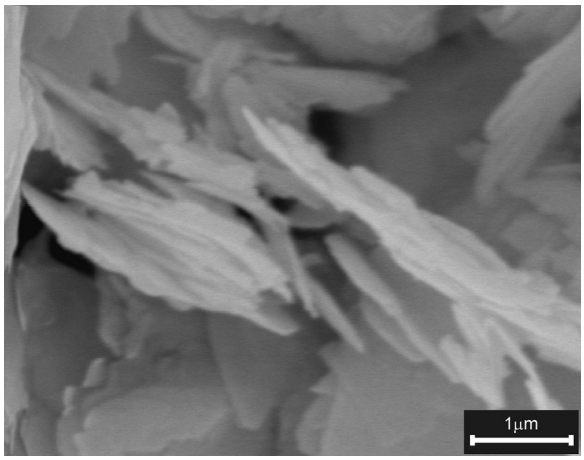


**Fig. 1.** SEM micrographs (20000×) of talc nanoparticles.

### 2.2. Thermoplastic starch mixtures

Blend composition as well as processing conditions were set following literature data for analogous systems processed by thermo-compression (Thunwall, Boldizar, & Rigdahl, 2006). Mixtures of native corn starch, glycerol (30%, w/w), distilled water (45%, w/w) and talc nanoparticles (0, 1.7, 5.2 and 8.7%, w/w) were prepared. Blend composition was expressed in g per 100 g of starch, which implies that 0, 1, 3 and 5%, w/w of talc, respect to TPS, were used. Talc was premixed with starch to achieve good particle dispersion between both powders. Then, glycerol and distilled water were added and samples were mixed and conditioned at 25 °C during 24 h. After that, conditioned mixtures were processed in a Brabender Plastograph (Brabender, Germany) at 140 °C and 50 rpm for 15 min. Processed mixtures were removed from the mixing chamber, triturated and conditioned at 25 °C and 60% relative humidity (RH), in order to improve their future proccesability. These ambient conditions were reached employing aqueous glycerol solutions at 72%, w/w.

### 2.3. Films preparation

Thermoplastic starch films were obtained by thermo-compression molding using a hydraulic press. Processing conditions were 150 kg cm$^{-2}$ at 140 °C during 6 min. An aluminum support as mold of 1 mm thickness and a molding relation of 3 g sample per cm$^3$ was used. The material was cooled under pressure up to approximately 50 °C; then the pressure was released and obtained films were removed from the molds. Before characterization, films were conditioned at 25 °C and 60% RH. The thickness of the films was measured at different locations of the specimens, employing a micrometer. Ten measurements were taken on each film and mean values are reported.

### 2.4. Structural aspects

#### 2.4.1. Fourier Transform Infrared Spectroscopy (FTIR)

Spectra were obtained using a Thermo Nicolet Nexus spectrophotometer (USA). Samples were prepared by mixing thermoplastic starch mixtures as fine powder with KBr (Sigma–Aldrich, 99%) at 3%, w/w. The mixture was pressed and a transparent sample was obtained. Spectra were obtained from 100 accumulated scans at 4 $cm^{-1}$ resolution in the range 4000–400 $cm^{-1}$.

#### 2.4.2. Scanning Electronic Microscopy (SEM)

Talc nanoparticles distribution and dispersion in the TPS matrix, as well as, homogeneity and appearance of the developed films were studied by SEM. On the other hand, a quali- and quantitative elemental analysis were done by using Dispersive Energy X-Ray Analysis. This study was performed in a JEOL JSM-35 CF electron microscope (Japan), with a secondary electron detector and a coupled microanalysis system EDAX 2000. Films were cryofractured by immersion in liquid nitrogen, mounted on bronze stubs and coated with a gold layer (~30 Å), using an argon plasma metallizer (sputter coater PELCO 91000). Thus, film surfaces and their cross-sections, as well as, Energy Dispersive X-Ray Spectroscopy (EDS) line scans were satisfactorily observed.

#### 2.4.3. X-ray diffraction (XRD)

Crystal structure identification of thermoplastic starch, crystallinity degree (CD) of TPS and degree of talc exfoliation were studied by XRD. Diffractograms of conditioned films were obtained in an X-ray diffractometer Philips PW1710 (Philips, Holland), provided with a tube, a copper anode, and a detector operating at 45 kV and 30 mA within $2\theta$ from 3 to 60°. Crystallinity degree of TPS matrixes was calculated as the ratio between the absorption peaks (without considering those corresponding to the talc) and the total diffractogram area, expressed as percentage (%). Besides, according to Bragg's equation, basal spacing of talc layers $d$ was obtained in order to evaluate the degree of exfoliation (Mbey, Hoppe, & Thomas, 2012).

#### 2.4.4. Transmission electron microscopy (TEM)

Dispersion of talc layers was analyzed by TEM. Samples were microtomed at room temperature using an ultramicrotome LKB Ultrotome 2088 (KB-Produkter AB., Bromma, Sweden) equipped with a diamond knife. Ultrathin sections (~1000 Å) were picked up using a copper grid. The samples were examined using a JEOL 100 CX (JEOL USA, Inc.) operating at an acceleration voltage of 100 kV.

### 2.5. Optical properties

#### 2.5.1. Opacity and UV barrier capacity

The absorbance spectrum (200–700 nm) was recorded using a SHIMADZU UV-160 (Japan) spectrophotometer. Films were cut into rectangles (3 cm × 1 cm) and placed on the internal side of a quartz spectrophotometer cell. Film opacity (AU nm) was defined as the area under the recorded curve determined by an integration procedure according to Piermaría, Bosch, Pinotti, Yantorno, García, & Abraham (2011) and the standard test method for haze and luminous transmittance of transparent plastics recommendations (ASTM D1003-00). The blocking effect of filler to UV transmission was calculated with the equation proposed by Sanchez-Garcia, Hilliou, and Lagaron (2010) as follows:

$$\text{Blocking effect} = \frac{(T_{\text{control}} - T_{\text{nanocomposite}})}{m_t} \quad (1)$$

where $T_{\text{control}}$ and $T_{\text{nanocomposite}}$ refer to percent transmittance for the TPS control film and the nanocomposite film, respectively and $m_t$ is the percent of talc with respect to starch mass.

The blocking effect was calculated for three wavelengths 300 nm, 350 nm and 750 nm in UV-B, UV-A and visible region, respectively (Mbey et al., 2012).

#### 2.5.2. Color measurements

Films color measurements were performed using a Hunterlab UltraScan XE (USA) colorimeter in the reflectance mode. Color parameters $L$, $a$, and $b$ were recorded according to the Hunter scale, in at least ten randomly selected positions for each film sample. Color parameters range from $L = 0$ (black) to $L = 100$ (white), $-a$ (greenness) to $+a$ (redness), and $-b$ (blueness) to $+b$ (yellowness). Standard values considered were those of the white background ($L = 97.75$, $a = -0.49$, and $b = 1.96$). Besides, $\Delta L$, $\Delta a$ and $\Delta b$ were calculated, taking into account the standard values of the white background and the parameter color difference was also determined as follows:

$$\Delta E = \sqrt{\Delta L^2 + \Delta a^2 + \Delta b^2} \quad (2)$$

### 2.6. Thermal properties and dynamic mechanical behavior

#### 2.6.1. Differential Scanning Calorimetry (DSC)

Thermal properties of TPS films were determined by DSC. A Perkin Elmer Pyris I (USA) calorimeter was used. Approximately 10 mg of film, previously conditioned at 25 °C and 60% RH were weighted in hermetic pans in order to avoid water loss. An empty hermetic pan was used as reference. Samples were heated from 20 to 250 °C at 10 °C/min, under nitrogen atmosphere. From these thermograms, the following parameters were obtained: onset ($T_0$), peak ($T_P$) and final ($T_F$) melting temperature and enthalpy of melting ($\Delta H$).

#### 2.6.2. Dynamic mechanical analysis (DMA)

Temperatures and intensities of relaxation phenomena for conditioned films were determined by DMA. Measurements were carried out in a dynamic-mechanical thermal equipment Q800 (TA Instruments, New Castle, USA) with a liquid nitrogen cooling system, using a clamp tension. Multi-frequency sweeps at fixed amplitude from −100 to 100 °C at 2 °C/min were carried out. Storage ($E'$) and loss ($E''$) moduli and tan $\delta$ curves as a function of temperature were recorded and analyzed using the software Universal Analysis 2000. $E'$ is related to the mechanical energy stored per cycle when the sample is subjected to deformation and it is the elastic response of the material. $E''$ is the viscous response which is related to the energy dissipated as heat per cycle when the sample is deformed. Loss factor is defined as $\tan\delta = E''/E'$, being $\delta$ the angle between the in-phase and the out-of-phase components of the modulus in the cyclic motion. Temperatures of the relaxation processes associated to glass transition temperatures ($T_g$) were determined through the inflexion point of the storage modulus $E'$ curve as well as the maximum peak in both the loss modulus $E''$ and tan $\delta$ curves (Psomiadou, Arvanitoyannis, & Yamamoto, 1996).

### 2.7. Statistical analysis

A completely randomized experimental design was used to characterize the nanocomposite films. Analysis of variance (ANOVA) was used to compare mean differences of samples properties. Besides, comparison of mean values was performed by Fisher's least significant difference test conducted at a significance level $p = 0.05$.

## 3. Results and discussion

### 3.1. Structural aspects

FTIR spectroscopy has been used for investigating changes in TPS structure on a short-range molecular level and to identify the potential interactions between starch, glycerol and talc nanoparticles. Fig. 2 shows the FTIR spectra corresponding to the TPS control matrix, talc, as well as, the nanocomposite with 5%, w/w talc. TPS spectrum presented bands corresponding to the distinctive functional groups of starch and glycerol. Bands at 920, 985, 1026, 1074 and 1148 $cm^{-1}$ (C–O stretching), 1648 $cm^{-1}$ (bound water), 2929 $cm^{-1}$ (C–H stretching), 3385 $cm^{-1}$ (–OH groups) and 1457 $cm^{-1}$ (glycerol) were detected according to Zhang and Han (2006). Besides, several bands at low wavenumbers (627, 581, 560 and 400 $cm^{-1}$) attributed to the complex vibrational modes due to skeletal mode vibrations of the glucose ring (Kizil, Irudayaraj, & Seetharaman, 2002) were observed. Regarding talc filler, characteristics bands were detected at 3676 $cm^{-1}$ ($Mg_3$-OH), 1019 $cm^{-1}$ (Si–O–Si stretching), 671 $cm^{-1}$ (–OH deformation), 536 and 452 $cm^{-1}$ (Si–O–Mg), 466 $cm^{-1}$ (Mg–O) and 426 $cm^{-1}$ (Si–O) as reported by Castillo et al. (2011). Nanocomposite spectrum presented the signals corresponding to TPS matrix as well as those to talc particles, as expected. However, slightly changes in the modes below 800 $cm^{-1}$ were observed. Similar results were reported by Wilhelm et al. (2003) studying clay addition influence on cará starch films structure. Besides, talc bands intensities in nanocomposite were relatively weak due to the low talc concentration.

SEM micrographs of criofractured surfaces of TPS films are shown in Fig. 3. In the case of the TPS film without talc particles (TPS control films) an homogenous appearance of the cross-section indicates the effectiveness of the thermo-compression process, where starch granules are not recognized (Fig. 3A). Besides, these films presented homogeneous and smooth surfaces. Since these films resulted transparent with absence of granules, they are useful for developing food packages where the product must be visible.

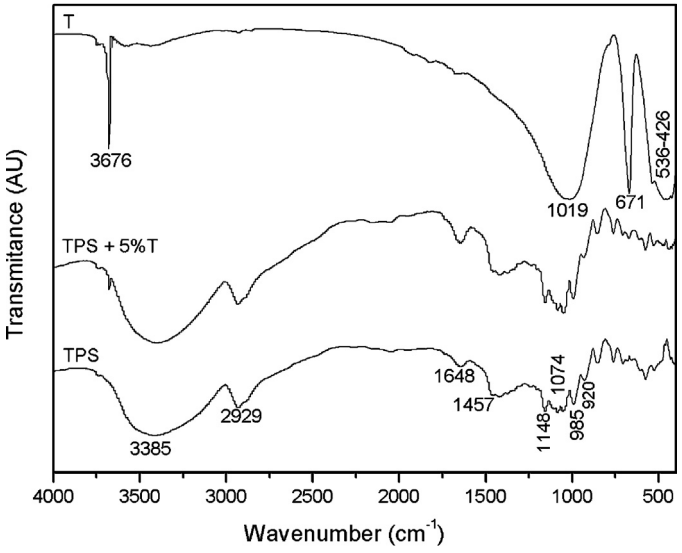


**Fig. 2.** FTIR spectra of talc and thermoplastic corn starch films with 0 and 5%, w/w nanoparticles.

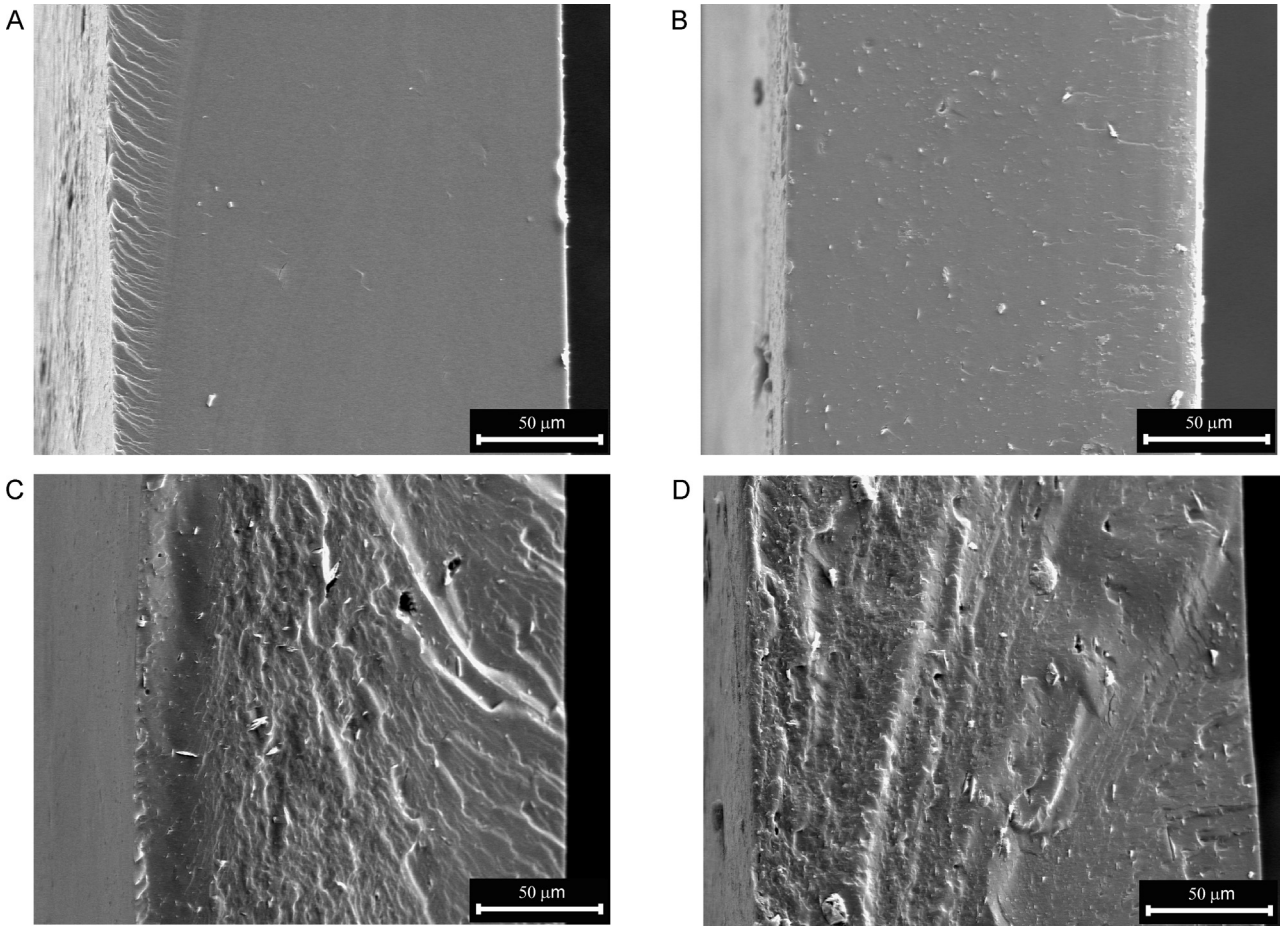


**Fig. 3.** SEM micrographs (540×) of thermoplastic corn starch films with (A) 0, (B) 1, (C) 3 and (D) 5%, w/w talc nanoparticles.

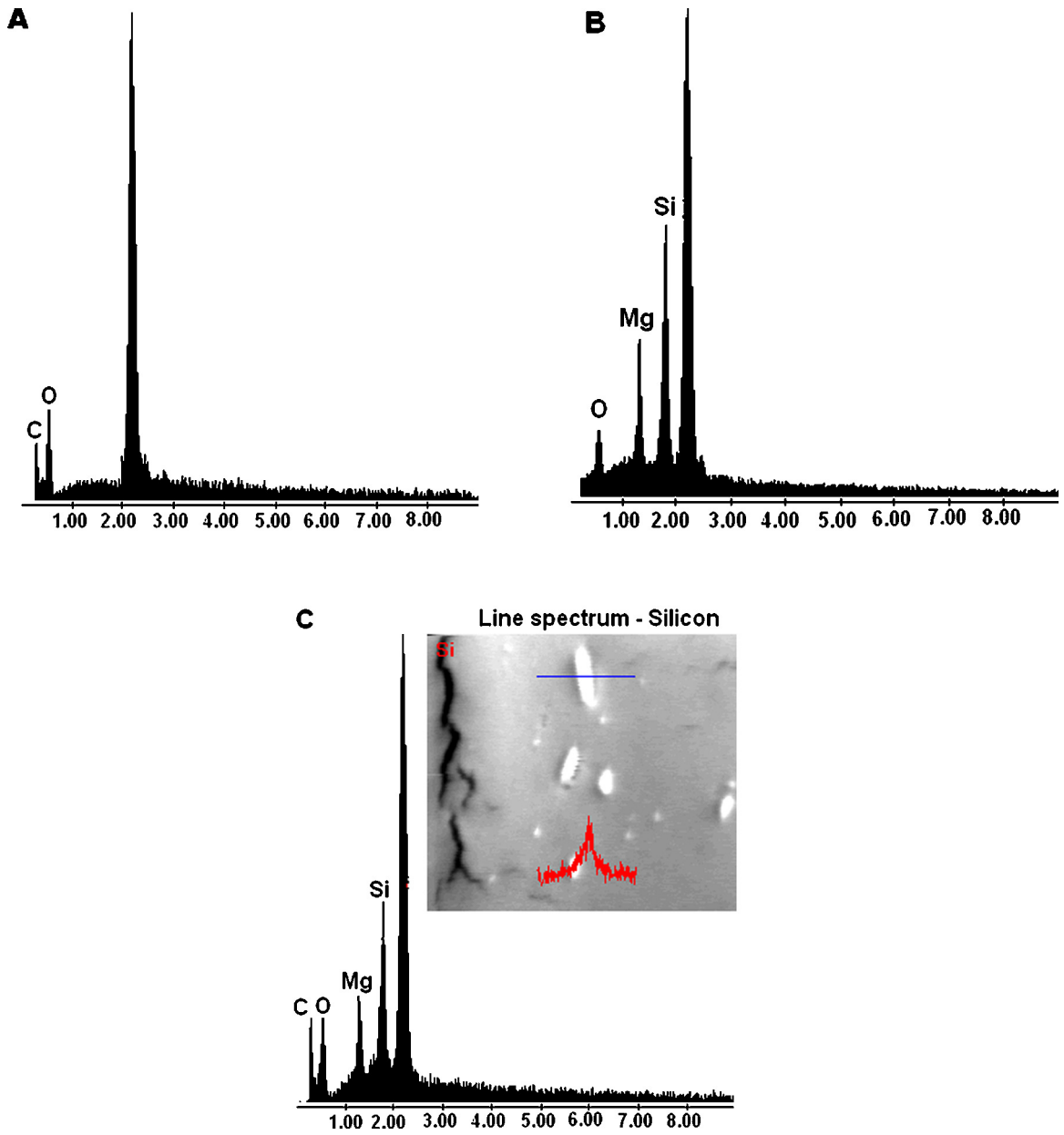


**Fig. 4.** EDX and line spectra of (A) thermoplastic corn starch films; (B) talc and (C) corn thermoplastic starch films with 1%, w/w talc nanoparticles.

Likewise, glycerol losses were negligible, since the processing temperature was kept well below the plasticizer boiling point. Thus, in all formulations no exudation was observed after processing.

Homogeneous films of TPS formulations with talc were also obtained by thermo-compression; with a good distribution and dispersion of nanoparticles in the TPS matrix (Fig. 3B–D). de Melo et al. (2011) stressed that starch-nanoclay films showed continuous matrixes, but their surfaces were less smooth than TPS films. The uniform dispersion of nanoparticles promotes a very large matrix/filler interfacial area, which changes the molecular mobility, the relaxation behavior and the consequent thermal and mechanical properties of the material (de Azeredo, 2009). Particle aggregation was not observed in SEM micrographs, evidencing at this scale, good filler dispersion within the matrix. Good adhesion for talc–TPS interfaces also indicates a good compatibility between particles and matrix, even for an unmodified surface mineral.

Particle preferential orientation was observed in the matrix for all talc concentrations, and it could be attributed to the filler laminar morphology which leads their alignment during the thermo-compression processing. On the other hand, talc incorporation modified the film fractured surface, increasing their irregularity with an increment of particle concentration (Fig. 3B–D). This observed result was expected since the addition of talc into TPS matrices increases the rigid phase of the material.

Fig. 4 presents EDS spectra corresponding to TPS matrix, talc particles, as well as, nanocomposite with 1%, w/w talc. The presence of C and O peaks was observed in the TPS spectrum (Fig. 4A). On the other hand, Si, Mg, as well as, O were detected in talc sample (Fig. 4B). For nanocomposites, the presence of talc particles was evident since elements constituents of this mineral were identified, as well as, those corresponding to TPS matrix (Fig. 4C). Profile of Si was performed on nanocomposite by EDS line scan mode. It can be observed that concentration of this element increased, as expected, when a talc particle was detected within the TPS matrix (Fig. 4C).

Quantitative information about TPS crystallinity changes was obtained from XRD spectra. Fig. 5 shows XRD patterns for pure

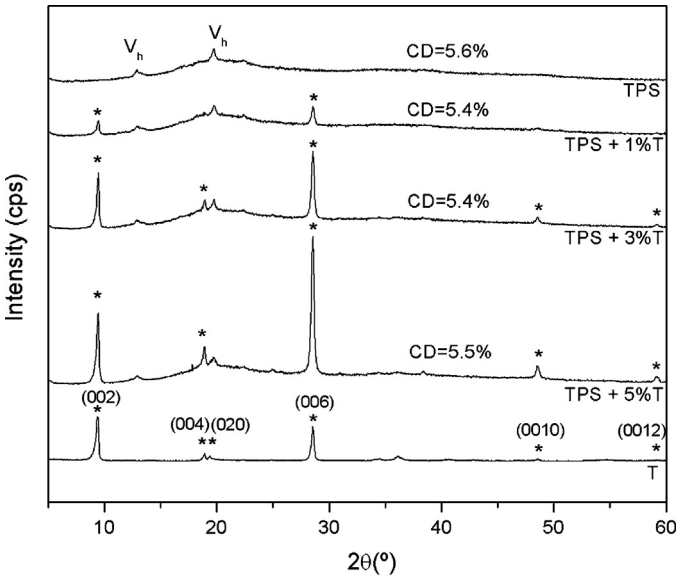


**Fig. 5.** XRD spectra of talc and thermoplastic corn starch films with 0, 1, 3 and 5%, w/w talc nanoparticles.

talc, TPS control films, as well as, TPS–talc nanocomposite films. Talc sample exhibited a well defined crystal structure, giving sharp (0 0 l) reflections as they are identified in Fig. 5. TPS spectrum presented low intensity, broad diffraction peaks and a large amorphous scattering halo. These characteristics correspond to a semi-crystalline polymer with low crystallinity (Fig. 5). The main reflection peaks which contributed to TPS crystallinity can be detected at 12.8° and 19.6° (Fig. 5). For thermoplastic corn starch with glycerol, Shi et al. (2006) reported the presence of two sharp peaks at 13.5° and 20.9° and assigned them to V-type structure. The V-type crystalline structure is formed by the crystallization of amylose in single helices involving glycerol or lipids and it can be divided into two subtypes, namely $V_a$ (anhydrous) with peaks at 13.2° and 20.6° and $V_h$ (hydrated) with peaks at 12.6° and 19.4° (Corradini, de Morais, Demarquette, Agnelli, & Mattoso, 2007). Yang, Yu, and Ma (2006) stressed that $V_h$-style crystallinity is induced by thermal processing where the strong interaction between hydroxyl groups of starch molecules was substituted by hydrogen bonds formed between plasticizer and starch during thermoplastic processing. Besides, clear evidence that native corn starch granules were destructed during processing was the absence of the reflection peaks corresponding to the A-type crystal structure, characteristic of cereal starches (Bader & Göritz, 1994; López et al., 2010a,b).

In the diffractograms of TPS–talc films, the reflection peaks corresponding to talc nanoparticles and those of the TPS matrix can be observed (Fig. 5). Crystalline structure of nanocomposite films resulted similar to that of TPS matrix. However, a slight decrease in the intensity and a widening in the peaks corresponding to the TPS matrix were observed in TPS–talc nanocomposites. This change was more evident at low scattering angles, especially in the peaks located at 12 and 19°, and for the formulation containing 5%, w/w talc. Ungar (2004) stressed that X-ray peak broaden indicates that crystal lattice has become imperfect, according to the theory of kinematical scattering, peak broadening is caused by either small crystal size or the presence of a large amount of lattice defects. Despite these slight changes observed in the spectrum of TPS, the addition of talc nanoparticles did not modify the degree of crystallinity of TPS matrix (Fig. 5). As it was expected, talc peaks intensity increased with nanoparticles concentration.

**Table 1**
Basal spacing of the talc (T) layers in thermoplastic corn starch films (TPS).

| Film formulation | $2\theta$ (°) | $d$ (Å) |
|---|---|---|
| TPS + 1% T | 9.49 | 9.32 |
| | 18.96 | 4.68 |
| | 19.73 | 4.50 |
| | 28.60 | 3.12 |
| | 48.60 | 1.87 |
| TPS + 3% T | 9.48 | 9.33 |
| | 18.97 | 4.68 |
| | 19.87 | 4.49 |
| | 28.58 | 3.12 |
| | 48.58 | 1.87 |
| TPS + 5% T | 9.47 | 9.34 |
| | 18.94 | 4.69 |
| | 19.77 | 4.49 |
| | 28.57 | 3.12 |
| | 48.56 | 1.87 |

For nanocomposite films, the $2\theta$ position of (0 0 l) talc peaks was similar to the corresponding value in the spectrum of talc sample (Table 1). As a consequence, interplanar basal spacing shifts were not observed, even for films with the lowest filler concentration studied (1%, w/w). However, other authors reported that some phyllosilicates, such as clays, can be exfoliated by the intercalation of polymer and plasticizer among layers (Wilhelm et al., 2003). In this work, results suggest that exfoliation of talc platelets did not occur at the processing conditions employed. Particularly, talc did not have exchangeable cations in the interplanar distance, restricting the possibility of talc exfoliation when it is mixed with TPS. On the other hand, clay has a notable cation exchange capacity allowing glycerol molecules intercalation by expanding intergallery spaces of the clay. Despite untreated nanoparticles used in this work, talc surface modification could be an alternative to overcome platelets exfoliation. Other alternative to allow talc nanoparticles intercalation and exfoliation in talc–TPS nanocomposites could be the processing method. Pandey and Singh (2004) showed that mixing order influences montmorillonite (MMT) interaction in samples containing starch, MMT, and glycerol, and they concluded that a better dispersion of MMT is generated when starch and MMT are mixed without glycerol. They attributed this to two reasons: first, electrostatic attraction between plasticizer and starch resulting in large structures stabilized by hydrogen bridges, negatively affecting starch chains mobility; and second, the formation of hydrogen bonds between starch and glycerol decreasing the attractive forces between starch and clay; with an increase in the extent of clay intercalation due to the extensive diffusion of polymer chains inside clay galleries.

In talc–TPS diffractograms, sharper (0 0 l) talc peaks were detected, evidencing the alignment of nanoparticles due to the thermo-compression process, this result was in agreement with SEM observations previously described (Fig. 3). This leads to the development of a more ordered talc structure in the TPS matrix. Similar results were reported by Chen and Evans (2005), studying composite films based on TPS and different clays. On the other hand, McGlashan and Halley (2003) working with starch-based composite materials reported that XRD investigations reveal that (0 0 1) peak for clay appears to be sharper with an increase in the amount of glycerol added; which means that intercalation is limited and a possible reason for this behavior could be that higher glycerol concentrations lead to stronger glycerol–starch interactions which limits the level of clay intercalation with clay–glycerol interactions. Besides, Pandey and Singh (2004) reported that composites obtained by extrusion, where a higher specific mechanical energy input is used, degradation of starch granules would lead to an increased dispersion of polymer chains within clay nanolayers.

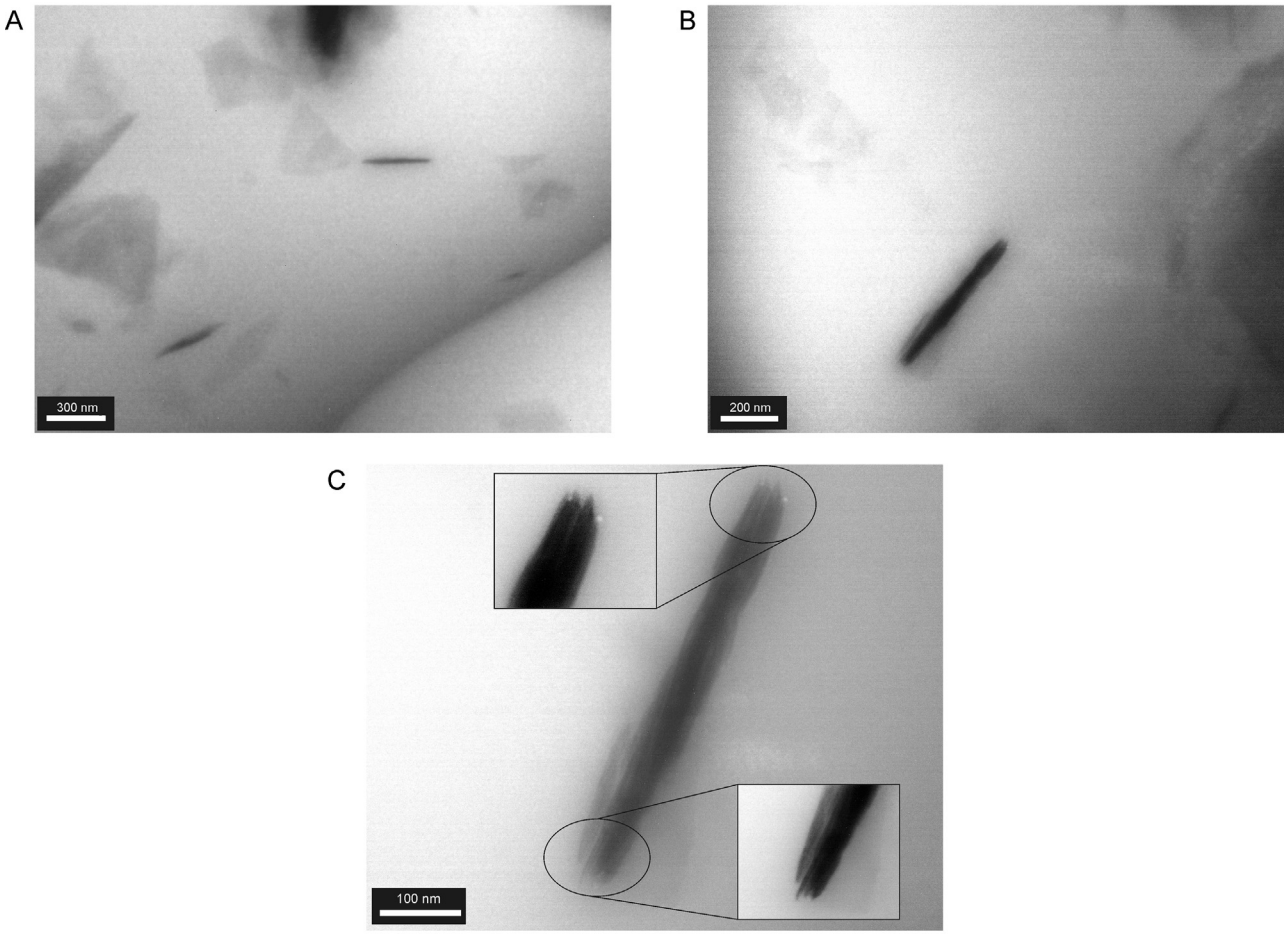


**Fig. 6.** TEM micrographs of thermoplastic corn starch films with 3%, w/w talc nanoparticles at different magnifications: (A) 50,000×, (B) 80,000× and (C) 200,000×.

This could be an additional reason for a low degree of exfoliation when a high concentration of plasticizer is used.

TEM observations gave a qualitative understanding of the internal structure, spatial distribution and dispersion of talc platelets within the TPS matrix through direct visualization. Fig. 6 shows representative TEM micrographs of TPS–talc nanocomposites containing 3%, w/w particles at different magnifications. Silicate layers were presented mostly as stacks of several platelets, although it was also observed some single platelets. The presence of a multilayered nanostructure of thick particles suggested the formation of talc agglomerates in the nanocomposites. Besides, it was evidenced that laminar morphology of the filler is extremely thin, demonstrating that used particles were in fact nano-sized filler.

TEM micrographs at low magnifications (Fig. 6A) showed a heterogeneous morphology, containing domains rich in talc nanoparticles and some regions without particles. This inhomogeneous distribution of filler in the TPS matrix was not evidenced in SEM micrographs neither by XRD analysis, thus emphasizing the importance of studying the structure using complementary techniques. Chivrac, Pollet, Schmutz, and Avérous (2008) have reported similar results for plasticized starch/MMT bionanocomposites. Avérous (2004) stressed that this result could be associated to the high glycerol content of the plasticized starch formulation, which induces a phase separation between domains with high and low glycerol content. TEM micrographs at higher magnifications (Fig. 6B–D) show the aggregates aforementioned and individual talc platelets randomly dispersed. The presence of individual particles seems to indicate that silanol groups of talc particle and hydroxyl groups of starch chains could interact by the formation of hydrogen bonds, favoring the nanofiller dispersion (Chivrac, Pollet, & Avérous, 2009). Fig. 6C and D corresponds to one of the particle stacks presented in the nanocomposites, showing an incipient intercalation of TPS matrix among talc platelets.

### 3.2. Optical properties

The evaluation of films optical properties is relevant since this is a key property for some applications such as packaging, among others. There was no significant difference ($p > 0.05$) among sample thickness, which varied from 196 to 214 μm. In this sense, thermocompression molding allows obtaining films with a controlled thickness, which is a very important parameter in the analysis of TPS–talc structure properties relationships.

Films color parameters are shown in Table 2. Talc nanoparticles modified TPS films luminosity, as well as, their chromaticity parameters ($a$ and $b$). The addition of talc concentration above 3%, w/w decreased significantly ($p < 0.05$) the luminosity of the TPS films. Besides, films with nanoparticles showed lower values ($p < 0.05$) of $a$ parameter (red–green), while $b$ parameter (yellow–blue) resulted significantly higher compared to TPS control films. Color differences ($\Delta E$), which shows the combined effects of the three color parameters ($a$, $b$, and $L$), are also presented in Table 2; the addition of 3%, w/w talc nanoparticles to the TPS matrixes modified significantly ($p < 0.05$) the $\Delta E$ value of the obtained films.

Fig. 7A corresponds to the UV–vis spectra of TPS films for all the talc concentrations studied. The evaluation of UV absorption capacity of developed films is relevant in order to propose possible applications of these materials, especially in the food packaging

**Table 2**
Color parameters and opacity of thermoplastic corn starch films (TPS) with talc nanoparticles (T).

| Film formulation | Color parameters | | | | Opacity (AU × nm) |
|---|---|---|---|---|---|
| | *L* (luminosity) | *a* (red–green) | *b* (yellow–blue) | $\Delta E$ | |
| TPS + 0% T | 85.4 ± 0.2[a] | 8.00 ± 0.02[a] | 1.6 ± 0.1[a] | 85.8 ± 0.2[a] | 31.8 ± 6.4[a] |
| TPS + 1% T | 85.0 ± 0.4[a,b] | 7.88 ± 0.06[b] | 2.1 ± 0.3[b] | 85.4 ± 0.5[a,b] | 54.5 ± 6.7[b] |
| TPS + 3% T | 84.5 ± 0.4[b] | 7.88 ± 0.05[b] | 2.4 ± 0.3[b] | 84.9 ± 0.5[b] | 71.6 ± 2.1[c] |
| TPS + 5% T | 83.1 ± 0.5[c] | 7.83 ± 0.05[b] | 4.3 ± 0.4[c] | 83.6 ± 0.6[c] | 109.0 ± 9.3[d] |

Reported values correspond to the mean ± standard deviation. Values within each column followed by different letters indicate significant differences ($p < 0.05$).

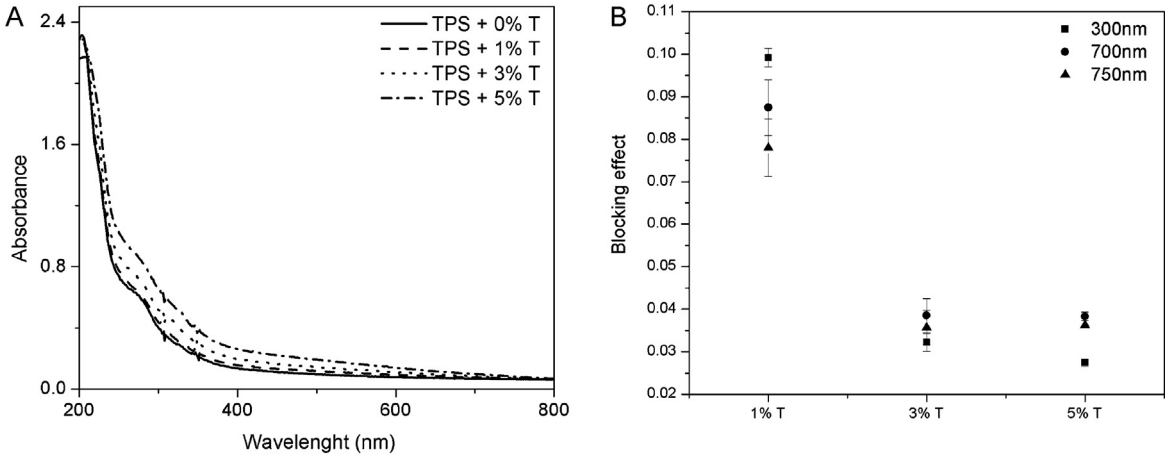


**Fig. 7.** (A) Absorption spectra (200–700 nm) and (B) blocking effect of thermoplastic corn starch films with 0, 1, 3 and 5%, w/w talc nanoparticles.

area. Films able to absorb in the UV zone could be useful to package and extend shelf life of food products which are susceptible to the oxidative rancidity catalyzed by UV light. Instead, films that are not able to absorb in this spectral region could be used to develop packages for food which must be later sanitized by UV light exposition to diminish their microbial charge. All the spectra shown in Fig. 8A presented an absorption peak located between 270 and 300 nm, indicating that talc nanoparticles did not affect the UV absorption capacity of TPS control films. Besides, this study allowed us to analyze the dispersion of filler in the matrix and to gather information on the blocking effect of talc to UV and visible radiation. The blocking effect is illustrated in Fig. 7B as a function of talc concentration. An increment in talc concentration from 1 to 3%, w/w led to a significant ($p < 0.05$) reduction of UV and visible light transmission. When talc is added to the TPS matrix, there is a reduction of transmittance in accordance with an increase in color development of the films, as previously described. Similar tendency was reported by Mbey et al. (2012) for cassava starch–kaolinite composite films.

Table 2 shows films opacity values for the studied nanocomposites which are calculated from the visible region (400–700 nm) of the absorption spectra presented in Fig. 7A. Film opacity increased significantly ($p < 0.05$) with an increase in talc concentration in TPS formulations. In spite of the observed increase, recorded values for TPS–talc films were low since the layered silicates are extremely thin, as it could be observed by TEM (Fig. 6A). Thus, when they are dispersed in the polymeric matrix, the nanocomposites resulted optically clear in the visible range.

Despite the inhomogeneous dispersion and distribution of nanoparticles in TPS matrixes, observed by TEM (Fig. 6A), optical properties resulted quite uniform throughout TPS–talc films, evidencing that size of "nano-agglomerates" is lower than UV and visible wavelengths.

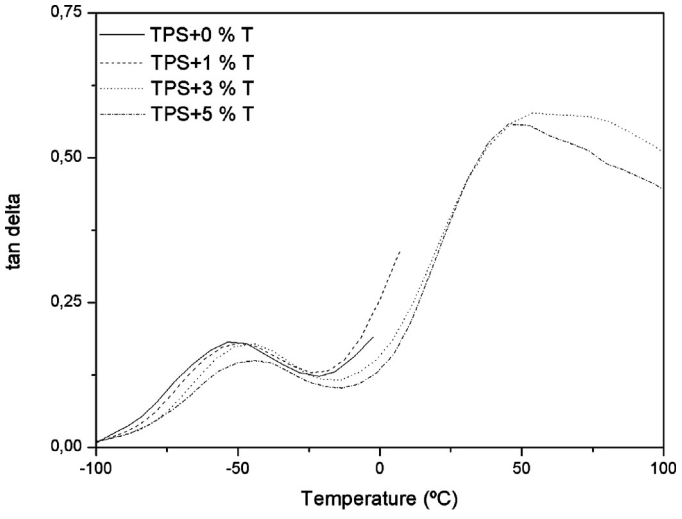


**Fig. 8.** DMA spectra of thermoplastic corn starch films with talc nanoparticles. Dependence of $E'$ (storage modulus), $E''$ (loss modulus) and tan $\delta$ with temperature at a constant frequency of 3 Hz.

### 3.3. Thermal properties and dynamic mechanical behavior

Analysis of thermal properties of materials by DSC is important in order to determine their processing temperature range and

**Table 3**
Thermal properties of thermoplastic corn starch films (TPS) with talc nanoparticles (T).

| Film formulation | Onset temperature (°C) | Melting temperature (°C) | Melting enthalpy (J/g TPS) |
|---|---|---|---|
| TPS + 0% T | 133.1 ± 1.3[a] | 156.4 ± 2.1[a] | 140.7 ± 32.2[a] |
| TPS + 1% T | 129.3 ± 3.6[a,b] | 148.2 ± 3.2[b] | 138.0 ± 20.2[a] |
| TPS + 3% T | 128.7 ± 2.6[b] | 146.0 ± 2.9[b] | 131.2 ± 9.2[a] |
| TPS + 5% T | 127.8 ± 3.1[b] | 144.3 ± 0.8[b] | 115.8 ± 17.3[a] |

Reported values correspond to the mean ± standard deviation. Values within each column followed by different letters indicate significant differences ($p < 0.05$).

**Table 4**
Relaxation temperatures associated to the glass transition of the glycerol- and starch-rich phases of thermoplastic corn starch films (TPS) with talc nanoparticles (T) determined by DMA (3 Hz).

| Film formulation | Relaxation temperatures associated to the glass transition of the glycerol-rich phase (°C) | | |
|---|---|---|---|
| | Inflexion of storage modulus ($E'$) | Maximum of loss modulus ($E''$) | Maximum of tan $\delta$ |
| TPS + 0% T | −68.0 ± 0.6[a] | −60.5 ± 4.1[a] | −51.8 ± 1.0[a] |
| TPS + 1% T | −67.3 ± 3.3[a] | −57.8 ± 5.8[a] | −51.2 ± 6.0[a] |
| TPS + 3% T | −53.7 ± 0.8[b] | −56.9 ± 0.8[a] | −47.1 ± 5.6[a] |
| TPS + 5% T | −55.1 ± 3.1[b] | −58.1 ± 3.0[a] | −45.4 ± 3.2[a] |
| Film formulation | Relaxation temperatures associated to the glass transition of the starch-rich phase (°C) | | |
| | Inflexion of storage modulus ($E'$) | Maximum of loss modulus ($E''$) | Maximum of tan $\delta$ |
| TPS + 0% T | nd | nd | nd |
| TPS + 1% T | nd | nd | nd |
| TPS + 3% T | 9.4 ± 0.7[a] | 30.0 ± 2.6[a] | 46.9 ± 0.8[a] |
| TPS + 5% T | 9.5 ± 0.8[a] | 28.8 ± 4.7[a] | 45.9 ± 0.8[a] |

Reported values correspond to the mean ± standard deviation. Values within each column followed by different letters indicate significant differences ($p < 0.05$). nd: no detected.

possible induced changes by talc in matrix cristallinity. All obtained TPS films exhibited a single endothermic transition, corresponding to the melting process of the crystalline phase of TPS matrix. Thermal parameters of TPS matrix and nanocomposites are presented in Table 3. Both onset and melting temperature corresponding to the nanocomposite films were lower than those of the TPS ones. This behavior was more significant at the higher talc content. The obtained results are in agreement with those acquired by XRD and they could be attributed to the presence of smaller and more irregular TPS crystals in nanocomposites than in control films. As a consequence, it is possible to conclude that talc acts as nucleating agent of TPS. These results agree with the assumption of Bhatnagar and Hanna (1996) for a similar system, and also with the well-known nucleating capability of talc for polypropylene matrixes (Castillo et al., 2012; Ferrage et al., 2002). There were no significant differences ($p > 0.05$) among melting enthalpy values (Table 3), in agreement with the lack of variation of crystallinity degree TPS matrix assessed by XRD (Fig. 5). However, these values presented a high data dispersion which could be attributed to the presence of two nanosized domains (starch and glycerol rich phases), previously observed by TEM (Fig. 6). Thus, mean entalphy values seem to decrease as the talc content increases related to the induction of smaller and more irregular crystals due to the talc nucleating effect.

Dynamic mechanical analysis provides information concerning the mechanical properties of solid polymeric systems, e.g. relaxation mechanisms, compatibility of polymer blends, damping properties and curing rate of polymeric systems (Demirgöz et al., 2000). Fig. 8 shows DMA spectra of TPS control film and those corresponding to nanocomposites. Several authors reported that starch–glycerol mixtures are partially miscible systems, given rise to a starch-rich phase and a glycerol-rich phase (Da Roz, Carvalho, Gandini, & Curvelo, 2006; García et al., 2009; López et al., 2011; Mathew & Dufresne, 2002). DMA curves of TPS films showed two relaxations, one located at lower temperatures which is associated to the glycerol-rich phase and the second one at a higher temperatures, associated to the starch-rich phase. In the case of TPS control films and the nanocomposite with 1%, w/w talc, relaxation corresponding to the starch-rich phase could not be determined since during the assays samples became soft (Fig. 8). However, it had been reported that the transition corresponding to the plasticizer-rich phase for different TPS matrixes has a better definition with a higher intensity change than the second one attributed to the starch-rich phase (Famá et al., 2006; Forssell, Mikkilä, Moates, & Parker, 1997; García et al., 2009; Hongsprabhas & Israkarn, 2008; Jiang, Qiao, & Sun, 2006; López et al., 2011; Ma et al., 2009; Wilhelm et al., 2003). An increase of rigid phase by addition of 3 and 5%, w/w talc nanoparticles to TPS matrix led to a higher softening resistance during measurements, allowing a better definition of the relaxation associated to the starch-rich phase for these nanocomposites (Fig. 8). In order to evaluate the effect of talc addition to TPS matrix, dynamic mechanical parameters were calculated. Relaxation temperatures associated to glass transitions of glycerol- and starch-rich phases for all developed TPS films are presented in Table 4. Despite there is no significant differences ($p > 0.05$) among relaxation temperatures corresponding to glycerol-rich phase, an increase in their mean values with talc concentration were observed. This tendency was found considering storage and loss moduli, as well as, tan $\delta$ curves and it could be attributed to chain mobility reduction due to the presence of talc nanoparticles. Similar results were reported by Chivrac et al. (2009) for the glass transition temperature of the starch rich phase of clay based starch composites. $T_g$ values corresponding to starch-rich phase of TPS and the nanocomposite with 1%, w/w talc films could not be assessed due to sample softening, as it was previously described. Relaxation temperatures of this phase for TPS films with 3 and 5%, w/w did not show significant ($p > 0.05$) differences between them (Table 4).

## 4. Conclusions

Nanocomposites films based on thermoplastic corn starch (TPS) and talc particles were prepared in order to evaluate the effect of filler addition on their structure, optical and thermal properties. Films were obtained by thermo-compression showing a good appearance and homogeneity in their thicknesses. FTIR spectrum corresponding to TPS was not modified with talc addition. TPS films presented homogeneous and smooth surfaces, observed by SEM. Talc addition increased the rigid phase of the developed materials, thus nanocomposite films fracture surfaces resulted more irregular than TPS ones. Laminar morphology of the used filler led to particle preferential orientation in the matrix during thermo-compression processing. A good compatibility between talc particles and TPS matrix was observed. Slight changes in the crystalline structure of TPS matrix with talc incorporation was obtained by XRD, mainly due to the nucleating effect of talc. This result was in agreement with the shifts on onset and peak temperatures observed by DSC. Despite these minor changes, talc addition did not modify TPS crystallinity degree, as it was measured by XRD and DSC. A more ordered talc structure in TPS matrix was evidenced by the presence of sharper (0 0 l) talc peaks in nanocomposites XRD spectra.

Randomly dispersed nano-agglomerates and individual platelets of talc were assessed by TEM. Besides, laminar morphology and nano-sized dimension of the filler were corroborated.

These talc characteristics made nanocomposite films optically transparent.

Partial miscibility of glycerol with starch was demonstrated by DMA. TPS films showed two relaxations, one associated to a glycerol-rich phase and the other to a starch-rich phase. Better definition of starch-rich phase relaxation in nanocomposites containing talc was achieved for concentrations higher than 3%, w/w since rigid phase was increased allowing higher softening resistance of these materials during DMA assays. Starch chains mobility was restricted due to the presence of talc nanoparticles, thus relaxation temperatures corresponding to glycerol-rich phase were shifted to higher values.

In summary, talc addition to native corn TPS matrix was analyzed by several and complementary techniques, focusing on films' structural changes, optical and thermal properties. Influence of talc incorporation on mechanical and barrier properties of TPS films is under study. Moreover, it is expected that these nanocomposite films could be used as promissory material for replacement of non biodegradable packaging films.

## References


Alexandre, M., & Dubois, P. (2000). Polymer-layered silicate nanocomposites: preparation, properties and uses of a new class of materials. *Materials Science and Technology*, *28*, 1–63.

Avérous, L. (2004). Biodegradable multiphase systems based on plasticized starch: A review. *Journal of Macromolecular Science Polymer Reviews*, *44*, 231–274.

Avérous, L., & Boquillón, N. (2004). Biocomposites based on plasticized starch: Thermal and mechanical behaviours. *Carbohydrate Polymers*, *56*(2), 111–122.

Avérous, L., & Frigant, C. (2001). Association between plasticized starch and polyesters: Processing and performances of injected biodegradable systems. *Polymer Engineering and Science*, *41*, 727–734.

Bader, H., & Göritz, D. (1994). Investigation on high amylose corn starch films. *Starch - Stärke*, *48*(3), 94–101.

Bhatnagar, S., & Hanna, M. (1996). Effect of talc on properties of corn starch extrudates. *Starch - Stärke*, *46*, 229–232.

Castillo, L., Barbosa, S., & Capiati, N. (2012). Influence of talc genesis and particle surface on the crystallization kinetics of polypropylene/talc composites. *Journal of Applied Polymer Science*, *126*, 1763–1772.

Castillo, L., Barbosa, S., Maiza, P., & Capiati, N. (2011). Surface modifications of talcs. Effects of inorganic and organic acid treatments. *Journal of Materials Science*, *46*, 2578–2586.

Chen, B., & Evans, J. (2005). Thermoplastic starch-clay nanocomposites and their characteristics. *Carbohydrate Polymers*, *61*, 455–463.

Chivrac, F., Pollet, E., & Avérous, L. (2009). Progress in nano-biocomposites based on polysaccharides and nanoclays. *Materials Science and Engineering Reports*, *67*, 1–17.

Chivrac, F., Pollet, E., Schmutz, M., & Avérous, L. (2008). New approach to elaborate exfoliated starch-based nanobiocomposites. *Biomacromolecules*, *9*, 896–900.

Corradini, E., de Morais, L., Demarquette, N., Agnelli, J., & Mattoso, L. (2007). Study of process parameters for starch, gluten, and glycerol mixtures. *Advanced Polymer Technology*, *18*, 861–867.

Cyras, V. P., Manfredi, L. B., Ton-That, M. T., & Vazquez, A. (2008). Physical and mechanical properties of thermoplastic starch/montmorillonite nanocomposite films. *Carbohydrate Polymers*, *73*, 55–63.

Da Roz, A., Carvalho, A., Gandini, A., & Curvelo, A. (2006). The effects of plasticizers on thermoplastic starch compositions obtained by melt processing. *Carbohydrate Polymers*, *63*, 417–424.

de Azeredo, H. (2009). Nanocomposites for food packaging applications. *Food Research International*, *42*, 1240–1253.

Demirgöz, D., Elvira, C., Mano, J., Cunha, A., Piskin, E., & Reis, R. (2000). Chemical modification of starch based biodegradable polymeric blends: Effects on water uptake, degradation behavior and mechanical properties. *Polymer Degradation and Stability*, *70*, 161–170.

de Melo, C., Salomao, G. P., Eiras, G. M., Yamashita, F., Dall'Antonia, L., & Mali, S. (2011). Properties of extruded xanthan-starch-clay nanocomposites films. *Barzilian archgives of Biology and Technology*, *54*, 1223–1333.

Famá, L., Flores, S., Gerschenson, L., & Goyanes, S. (2006). Physical characterization of cassava starch biofilms with special reference to dynamic mechanical properties at low temperatures. *Carbohydrate Polymers*, *66*, 8–15.

Ferrage, E., Martin, F., Boudet, A., Petit, S., Fourty, G., Jouffret, F., Micoud, P., De Parseval, P., Salvi, S., Bourgerette, C., Ferret, J., Saint-Gerard, Y., Buratto, S., & Fortune, J. (2002). Talc as nucleating agent of polypropylene: Morphology induced by lamellar particles addition and interface mineral-matrix modelization. *Journal of Materials Science*, *37*, 1561–1573.

Fornes, T., & Paul, D. (2003). Crystallization behavior of nylon 6 nanocomposites. *Polymer*, *44*, 3945–3961.

Forssell, P., Mikkilä, J., Moates, G., & Parker, R. (1997). Phases and glass transition behaviour of concentrated barley starch–glycerol–water mixtures, a model for thermoplastic starch. *Carbohydrate Polymers*, *34*, 275–282.

García, M., Martino, M., & Zaritzky, N. (2000). Lipid addition to improve barrier properties of edible starch-based films and coatings. *Journal of Food Science*, *65*, 941–947.

García, M., Pinotti, A., Martino, M., & Zaritzky, N. (2009). *Edible films and coatings for food applications*. New York: Springer. (Chapter 6)

Halley, P., Rutgers, R., Coombs, S., Kettels, J., Gralton, J., & Christie, G. (2001). Developing biodegradable mulch films from starch-based polymers. *Starch - Stärke*, *53*(8), 362–367.

Hongsprabhas, P., & Israkarn, K. (2008). New insights on the characteristics of starch network. *Food Research International*, *41*, 998–1006.

Jiang, W., Qiao, X., & Sun, K. (2006). Mechanical and thermal properties of thermoplastic acetylated starch/poly(ethylene-co-vinyl alcohol) blends. *Carbohydrate Polymers*, *65*, 139–143.

Kizil, R., Irudayaraj, J., & Seetharaman, K. (2002). Characterization of irradiated starches by using FT-Raman and FTIR Spectroscopy. *Journal of Agricultural and Food Chemistry*, *50*, 3912–3918.

Lagaron, J., & López-Rubio, A. (2011). Nanotechnology for bioplastics: Opportunities, challenges and strategies. *Trends in Food Science & Technology*, *22*, 611–661.

López, O., García, M., & Zaritzky, N. (2008). Film forming capacity of chemically modified corn starches. *Carbohydrate Polymers*, *73*, 573–581.

López, O., García, M., & Zaritzky, N. (2010a). Novel sources of edible films and coatings. *Postharvest Review*, *6*(3), 1–8.

López, O., García, M., & Zaritzky, N. (2010b). Physicochemical characterization of chemically modified corn starches related to rheological behavior, retrogradation and film forming capacity. *Journal of Food Engineering*, *100*(1), 160–168.

López, O., Lecot, C., Zaritzky, N., & García, M. (2011). Biodegradable packages development from starch based heat sealable films. *Journal of Food Engineering*, *105*(2), 254–263.

Ludueña, L., Alvarez, V., & Vasquez, A. (2007). Processing and microstructure of PCL/clay nanocomposites. *Materials Science and Engineering A*, *460–461*, 121–129.

Ma, X., Chang, P., Yu, J., & Stumborg, M. (2009). Properties of biodegradable citric acid-modified granular starch/thermoplastic pea starch composites. *Carbohydrate Polymers*, *75*, 1–8.

Mali, S., Karam, L., Pereira Ramos, L., & Grossmann, M. (2004). Relationships among the composition and physicochemical properties of starches with the characteristics of their films. *Journal of Agricultural and Food Chemistry*, *52*, 7720–7725.

Mali, S., Sakanaka, L., Yamashita, F., & Grossmann, M. (2005). Water sorption and mechanical properties of cassava starch films and their relation to plasticizing effect. *Carbohydrate Polymers*, *60*, 283–289.

Mathew, A., & Dufresne, A. (2002). Morphological investigation of nanocomposites from sorbitol plasticized starch and tunicin whiskers. *Biomacromolecules*, *3*, 609–617.

Mbey, J., Hoppe, S., & Thomas, F. (2012). Cassava starch–kaolinite composite film. Effect of clay content and clay modification on film properties. *Carbohydrate Polymers*, *88*, 213–222.

McGlashan, S., & Halley, P. (2003). Preparation and characterisation of biodegradable starch-based nanocomposite materials. *Polymer International*, *52*, 1767–1773.

Müller, C., Laurindo, J., & Yamashita, F. (2009). Effect of cellulose fibers addition on the mechanical properties and watervapor barrier of starch-based films. *Food Hydrocolloids*, *23*, 1328–1333.

Pandey, J., & Singh, R. (2004). Green nanocomposites from renewable resources: Effect of plasticizer on the structure and material properties of clay-filled starch. *Starch - Stärke*, *57*, 8–15.

Parra, D., Tadini, C., Ponce, P., & Lugão, A. (2004). Mechanical properties and water vapor transmission in some blends of cassava starch edible films. *Carbohydrate Polymers*, *58*, 475–481.

Piermaría, J., Bosch, A., Pinotti, A., Yantorno, O., García, M. A., & Abraham, A. (2011). Kefiran films plasticized with sugars and polyols: water vapor barrier and mechanical properties in relation to their microstructure analyzed by ATR/FT-IR spectroscopy. *Food Hydrocolloids*, *25*, 1261–1269.

Pinto, C., Carbajal, G., Wypych, A., Ramos, L., & Satyanarayana, K. (2009). Studies of the effect of molding pressure and incorporation of sugarcane bagasse fibers on the structure and properties of polyhydroxybutyrate. *Composites Part A Applied Science and Manufacturing*, *40*(5), 573–582.

Psomiadou, E., Arvanitoyannis, I., & Yamamoto, N. (1996). Edible films mnade from natural resources; microcrystalline cellulose (MCC), methylcellulose (MC) and corn starch and polyols: Part 2. *Carbohydrates Polymers*, *31*, 194–204.

Sanchez-Garcia, M., Hilliou, L., & Lagaron, J. (2010). Nanobiocomposites of carrageenan, zein, and mica of interest in food packaging and coating applications. *Journal of Agricultural and Food Chemistry*, *58*, 6884–6894.

Shi, R., Liu, Q., Ding, T., Han, Y., Zhang, L., Chen, D., & Tian, W. (2006). Ageing of soft thermoplastic starch with high glycerol content. *Journal of Applied Polymer Science*, *103*, 574–586.

Tapia Blácido, D., Sobral, P., & Menegalli, F. (2005). Development and characterization of biofilms based on Amaranth flour (*Amaranthus caudatus*). *Journal of Food Engineering*, *67*, 215–223.

Tunjano, V., Salcedo, F., Jiménez, I., Medina, J., Alvarez, O., & Prieto, E. (2009). Estudio de las propiedades térmicas y mecánicas del almidón termoplástico (TPS) reforzado con nanoarcilla. *Suplemento de la Revista Latinoamericana de Metalurgia y Materiales*, *1*, 29–36.

Thunwall, M., Boldizar, A., & Rigdahl, M. (2006). Compression molding and tensile properties of thermoplastic potato starch materials. *Biomacromolecules*, *7*, 981–986.

Ungar, T. (2004). Microstructural parameters from X-ray diffraction peak broadening. *Scripta Materialia*, *51*, 777–781.

Wilhelm, H., Sierakowski, M., Souza, G., & Wypych, F. (2003). Starch films reinforced with mineral clay. *Carbohydrate Polymers*, *52*, 101–110.

Yang, J., Yu, J., & Ma, X. (2006). Study on the properties of ethylenebisformamide and sorbitol plasticized corn starch (ESPTPS). *Carbohydrate Polymers*, *66*(1), 110–116.

Zhang, Y., & Han, J. (2006). Mechanical and thermal characteristics of pea starch films plasticized with monosaccharides and polyols. *Journal of Food Science*, *71*, 109–111.